Topology-Preserving Multi-Label Image Segmentation

Jarrell Waggoner[1], Youjie Zhou[2], Jeff Simmons[3], Marc De Graef[4], Song Wang[2]

[1]Groupon, Inc.; [2]Computer Science & Engineering, University of South Carolina;

[3]Materials and Manufacturing Directorate, AFRL; [4]Materials Science and Engineering, Carnegie Mellon University

jwaggoner@groupon.com zhou42@email.sc.edu, jeff.simmons@wpafb.af.mil,

degraef@cmu.edu, songwang@cec.sc.edu

Abstract

*Enforcing a specific topology in image segmentation is a very important but challenging problem, which has attracted much attention in the computer vision community. Most recent works on topology-constrained image segmentation focus on binary segmentation, where the topology is often described by the connectivity of both foreground and background. In this paper, we develop a new multi-labeling method to enforce topology in multi-label image segmentation. In this case, we not only require each segment to be a connected region (*intra-segment topology*), but also require specific adjacency relations between each pair of segments (*inter-segment topology*). We develop our method in the context of segmentation propagation, where a segmented template image defines the topology, and our goal is to propagate the segmentation to a target image while preserving the topology. Our method requires good spatial structure continuity between the template and the target such that the template segmentation can be used as a good initialization for segmenting the target. In addition, we focus on multi-label segmentation where a segment and its adjacent segments form a ring structure, which is among the most complex type of inter-segment topology for 2D structures. We apply the proposed method to segment 3D metallic image volumes for the underlying grain structures and achieve better results than several comparison methods. Finally, we also apply the proposed method to interactive segmentation and stereo matching applications.*

1. Introduction

Topology is a very important prior for many applications. In medical imaging [11, 15], different organs or tissues in the human body may show specific contextual relations. In materials science [14, 3], polycrystalline materials are usually made up of numerous grains with specific adjacency relations. Enforcing topology in image segmentation can substantially improve the segmentation accuracy and reliability [4, 6, 7, 10, 19, 9, 13, 17, 20].

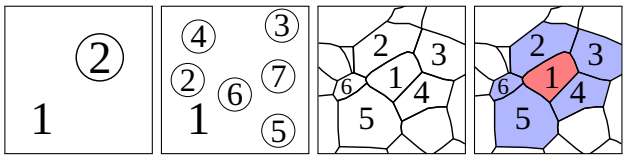

Figure 1: Examples of topology in segmentation. **(a)** Foreground/background segmentation, which has no inter-segment topology. **(b)** Simple inter-segment topology, showing few adjacency relationships among segments. **(c)** Complex inter-segment topology, with many and varied adjacency relationships between segments. **(d)** Example of a ring structure with segment 1 (red) as the ring center, and its immediate neighbors (blue).

One of the most widely used image segmentation models is the Markov Random Field (MRF), where the cost function contains a unary term for each individual pixel and a binary term for pixel pairs. In particular, many efficient algorithms, such as graph cut, have been used to solve the MRF optimization problem and derive an image segmentation.

Enforcing topology in an MRF-based image segmentation has attracted much attention in recent years [17, 19, 13, 4]. However, even the state-of-the-art work has only focused on the simple case of foreground/background (binary) segmentation, as shown in Fig. 1 (a). In this special case, the topology of such a segmentation is defined solely in terms of the connectivity of the foreground and/or background segments. We refer to such topology as *intra-segment topology*.

In practice, however, most applications require the segmentation of multiple structures of interest. The goal of topology preservation in this general case is to obtain multiple segments (> 2) such that each segment is a single connected region (intra-segment topology), and each pair of segments has pre-specified (non-)adjacency relations, i.e., *inter-segment topology*. Enforcing multi-segment topol-

978-1-4799-6683-7/15 $31.00 © 2015 IEEE
DOI 10.1109/WACV.2015.149

ogy in MRF-based image segmentation is of substantially greater complexity compared with binary segmentation. Even without considering the segmentation topology, MRF-based multi-labeling segmentation is NP-hard [16] and only locally-optimal solutions can be obtained.

In this paper, we develop a new approach to enforce both intra-segment and inter-segment topology in MRF-based multi-label segmentation. In practice, multi-segment topology may show different levels of complexity. In the most simple case, there is a single background segment, and all other segments neigbor this background segment, as shown in Fig. 1 (b). In this paper, we focus on one of the most complex multi-segment topologies, as shown in Fig. 1 (c), where each segment has multiple neighboring segments.

To make this challenging problem tractable, we introduce one simplification. To segment a target image, we assume a similar segmented template image is available which both defines the topology of the segmentation that we wish to preserve, and provides an initialization for the segmentation on the target. This simplification is reasonable for a number of applications, including 3D volume segmentation by propagating a 2D segmentation slice-by-slice, and segmentation propagation from one image to another collected for stereo matching.

To preserve the inter-segment topology, we independently consider each subset of segments that form a ring structure, as illustrated in Fig. 1 (d), which consists of a center segment and its immediate neighbors. We map these ring structures to the target image by incorporating the underlying image information into the binary term and conduct an MRF-based segmentation within each ring structure. By encoding non-adjacency constraints in the binary term, we show that the adjacency constraints are implicitly satisfied in a ring structure. To preserve the intra-segment topology, we set the unary term at each pixel to be to either 0 or ∞, determined by the spatial proximity to the segmentation boundaries in the template image. To evaluate the performance of the proposed method, we apply it to segment 3D metallic image volumes slice-by-slice for the underlying grain structures, and quantitatively compare its performance to several existing state-of-the-art methods. Finally, we also apply the proposed method to interactive segmentation and stereo matching applications.

2. Related Work

Intra-segment topology (i.e., segment connectivity) has been incorporated into MRF-based segmentation using graph-cut algorithms [17, 19, 13, 4] and level sets [7]. More specifically, in [17] a DijkstraGC algorithm was developed to enforce segment connectivity using interactively-specified points. In [13], a more general approach was developed to optimize the MRF cost function using a series of LP relaxations, with additional checks for segment connectivity. In [19], a Topology Cut algorithm was developed to insure segment connectivity in a MRF. In [4], a TopoCut algorithm achieves the desired intra-segment topology by modifying the underlying MRF before applying the graph-cut algorithm to minimize the cost function. This algorithm guarantees that the chosen connectivity property is preserved without explicitly enforcing it in the cost minimization and without using any kind of initialization. All these methods are formulated for binary segmentation with two labels: foreground and background.

Inter-segment topology involves more than two segments (labels). In [20], a topology-preserving algorithm is designed to work with a small collection of semantic segments which can encode spatial relationships between objects using a quadratic programming approach on a conditional random field (CRF). In [6], Watershed Cut, a variant of watershed, is proposed that better fits the segmentation to local regions in an image by removing "destructible" points during a morphological operation. In [9], image edges are identified without small gaps or other properties that may result in topological inconsistencies, as determined by a learning algorithm. In [10], a combination of region merging and an edge map is used to integrate a consistent homolology measure to roughly enforce the "complexity" of the resulting segmentation using the Betti number during the merging process. These works tend to enforce a more general notion of topology and do not allow arbitrary (non-)adjacency constraints to be specified, or only handle a very small number of segments for which the topology is enforced.

Related to the proposed work is the propagation method introduced in [18], which is developed for multi-label segmentation. In this method, the binary term in the MRF cost function is defined such that an infinity penalty is introduced when non-adjacent segments become adjacent. This way, it is guaranteed that non-adjacent segments cannot become adjacent in the segmentation propagation. However, it cannot guarantee that each segment remains connected, nor does it guarantee that two adjacent segments remain adjacent after the propagation.

3. Proposed Method

3.1. Propagation and Segmentation Topology

For ease of explanation, we formulate this problem as a segmentation propagation process [1]: given a segmentation S^U on the template image U, we wish to find the segmentation S^V on the target image V while preserving topology. U and V show good spatial structural continuity and we focus on multi-label segmentations, i.e., $|S^U| = |S^V| > 2$, in this paper.

[1] We can just as easily formulate this as an interactive segmentation, where the initialization S^U is supplied by a human instead of being the template for a propagation, as we show later in the experiments.

The inter-segment topology is defined by the pairwise adjacency relations among all the segments, i.e.,

$\{S_i, S_j\} \in \mathcal{A}$ iff S_i and S_j are adjacent in segmentation S.

Two segmentations have the same inter-segment topology if they contain same segment labels and the segments (labels) in these two segmentations show the same adjacency relations.

In [18], an MRF cost function $E(S^V)$ is defined for modeling segmentation propagation

$$E(S^V) = \sum_{p \in V} \Theta_p(S_i^V) + \sum_{\{p,q\} \in \mathcal{N}^V} \Phi_{pq}(S_i^V, S_j^V), \quad (1)$$

where $\mathcal{N}^V$ defines the spatial neighborhood in V. The unary term Θ_p is defined to reflect the spatial structure continuity between U and V within a fixed distance d of the initialization, i.e.,

$$\Theta_p(S_i^V) = \begin{cases} 0, & \text{distance}(p, S_i^U) < d \\ \infty, & \text{otherwise} \end{cases}. \quad (2)$$

This definition of Θ_p, using only 0 and ∞, preserves the intra-segment topology as discussed later in Section 3.3. The binary term is defined by

$$\Phi_{pq}(S_i^V, S_j^V) = \begin{cases} 0, & i = j \\ \infty, & \{S_i^U, S_j^U\} \notin \mathcal{A}^U \\ g(p,q), & \{S_i^U, S_j^U\} \in \mathcal{A}^U, \end{cases} \quad (3)$$

where $g(p,q)$ is derived from the intensity map in V which causes the segmentation boundary to pass through edge pixels, e.g.,

$$g(p,q) = \exp\left(-\beta \max(V(p), V(q))^2\right) \quad (4)$$

for edge images and

$$g(p,q) = \exp\left(-\beta (V(p) - V(q))^2\right) \quad (5)$$

for intensity images, where β is the multiplicative inverse of the expectation of the image intensity [2]. The major contribution in Eq. (3) is the infinity penalty when $\{S_i^U, S_j^U\} \notin \mathcal{A}^U$. This disallows any non-adjacent segments in U from becoming adjacent when propagated to V, i.e.,

$$\{S_i^U, S_j^U\} \notin \mathcal{A}^U \Longrightarrow \{S_i^V, S_j^V\} \notin \mathcal{A}^V.$$

Eq. (1) is a standard MRF cost function and can be locally minimized over the entire image V by repeated α-β swaps [1].

However, the above model introduced in [18] does not penalize the case where two adjacent segments in U become non-adjacent in V after propagation. Thus, it is not a segmentation propagation that enforces full topology preservation. In the following, we introduce a new algorithm to address topology preservation.

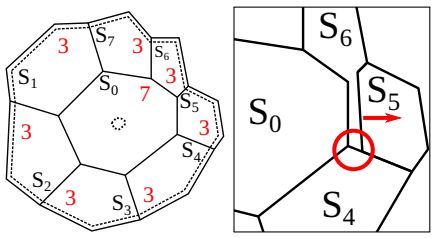

(a) (b)

Figure 2: Local ring structure example. **(a)** Preserving inter-segment topology by fixing the label of pixels along the ring boundary and in the center segment (dashed lines). Red numbers indicate the numbers of segments adjacent to the indicated segment. **(b)** Cropped view of (a) illustrating the preservation of inter-segment topology while updating the ring.

3.2. Inter-segment Topology

In this section, we propose an algorithm to propagate a segmentation by preserving full inter-segment topology, i.e., both adjacency and non-adjacency, which can be expressed as

$$\{S_i^U, S_j^U\} \in \mathcal{A}^U \iff \{S_i^V, S_j^V\} \in \mathcal{A}^V.$$

We achieve this by repeatedly updating the local ring structures sequentially. As illustrated in Fig. 2 (a), using the segmentation S^U as the initial segmentation on V, we find a local ring structure that consists of one center segment and all segments adjacent to this center segment. The center segment is adjacent to every non-center segment in the ring, and is not adjacent to any segments outside of the ring. Additionally, in the general case, each non-center segment has a clockwise adjacent segment and a counterclockwise adjacent segment other than the center segment in the ring. We also require the existence of at least one pair of non-adjacent segments in a ring to activate the infinity penalty as defined in Eq. (3). This leads to the requirement that there be at least 4 non-center segments in a ring. If a ring contains only 2 or 3 non-center segments, as shown in Fig. 3 (b)-(c), we can split one or two non-center segments along the radial direction, as shown in Fig. 3 (d)-(e), to increase the number of non-center segments and introduce non-adjacency. This updates S^U which is then propagated to V, after which we merge such split segments together to obtain the final segmentation S^V. Another degenerate case is when there is a single non-center segment in the ring, as shown in Fig. 3 (a), which reduces to the binary segmentation problem, and the method developed below can handle this degenerate case without splitting any segments.

From such a local ring structure, together with the image V on which this ring is embedded, we can define a MRF model (Eq. (1)) specifically within this ring, which we minimize to obtain an updated segmentation. The pri-

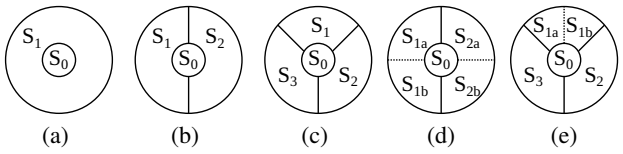

Figure 3: Illustration of the degenerate cases of ring structures. (a-c) Ring structures with 1, 2, and 3 non-center segments, respectively. (d-e) Non-center segment splitting to achieve four non-center segments for the rings in (b) and (c), respectively.

mary issue is that we must preserve the topology of all the segments in S^U, not simply the topology inside this ring. Therefore, we fix the labels for all the pixels along the ring boundary, shown by the dashed contour in Fig. 2 (a), e.g., the outer ring boundary shared with segment S_1 must still be labeled as S_1 after the update, etc. This can be easily achieved by assigning unary-term values for such pixels to be zero if their labels are the same as before and infinity otherwise. This way, we insure that the adjacency relations between any segment in this ring and any segment outside this ring will remain unchanged after the labeling update in this ring. To avoid the disappearance of the center segment, we also select the centroid pixel of the center segment and require its label to be unchanged (dashed lines in the center of Fig. 2 (a)).

Based on this, we simply use the MRF model with the binary term as defined in Eq. (3) within the image region defined by this ring to update its segmentation. As discussed above, this algorithm guarantees that non-adjacent segments remain non-adjacent. Which, together with the constraints defined on the ring boundary, will also guarantee that adjacent segments in this ring remain adjacent. This is indeed the case because, 1) the adjacency between non-center segments has been preserved by the label constraints on the ring boundary, and 2) the center segment is still adjacent to every non-center segment. For 2), it can be proved by contradiction, as shown in Fig. 2 (b). If the center segment S_0 becomes non-adjacent from a non-center segment, S_5, a pair of non-adjacent segments, S_4 and S_6 (be reminded that there are at least four non-center segments in a ring), must become adjacent to separate S_0 and S_5. However, the proposed algorithm has an infinity penalty term in Eq. (3) specifically to prevent any non-adjacent segments from becoming adjacent.

3.3. Intra-segment Topology

It is well known that most algorithms, including graph cut algorithms, that are developed to optimize an MRF cost function, may not guarantee the connectivity of each labeled segment. In this section, we show that this is not an issue for the proposed method. Our particular formulation, which uses 0 and ∞ for the unary term (see Eq. (2)), guarantees connectivity of each labeled segment. This can be illustrated by the example shown in Fig. 4. By using the Θ term as defined by Eq. (2), a "band" region (bounded by the two dashed lines) of width $2d$ will be defined around the initial segmentation boundary (black line). Pixels in this band region can be labeled as segment 1 or 2, with 0 unary cost. After optimization (α-β swap), the new boundary (red line) separating these two labels must be located within this band region. Otherwise, this would introduce an ∞ unary cost. If any segment, say segment 2 in this example, is disconnected, such a disjoint fragment (red circle) must also be in this band region to avoid ∞ unary cost. However, such a fragment will not appear in practice since the α-β swap will automatically merge this fragment (red circle) into its containing segment 1 which leads to a smaller binary cost, and therefore a lower total MRF energy (unary cost is always 0 and does not change before or after the α-β swap).

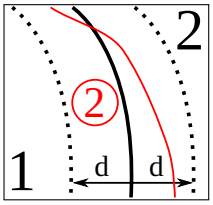

Figure 4: Illustration of segment connectivity in the proposed method.

With this formulation, we repeat the above steps for each local ring structure defined in S^U to update all segments. We may repeat the whole process for multiple rounds to continue updating the segment boundaries until they converge or until it reaches a pre-set maximum number of iterations. In practice we use a single iteration for all our experiments. Because we preserve the inter-segment topology and intra-segment topology of the entire segmentation while updating the segmentation in each local ring structure, it is easy to see that the complete iterative algorithm preserves both forms of topology at every step. As in the general multi-labeling problem, which is known to be NP-hard [16], our algorithm converges to a local minimum. Note that although we fix the ring boundary and its pixel labels in each step of segmentation update, this ring boundary and its pixel labels will be updated when taking other segments as the center of the ring, as shown in Fig. 5.

4. Experiments

In this section, we apply the proposed topology-preserving method to segment 3D electron microscopy metallic images to obtain their underlying grain structures, and show its application to interactive segmentation and stereo matching. For grain segmentation, we manually construct a grain segmentation on one slice as the initial template and then use the proposed method to propagate the

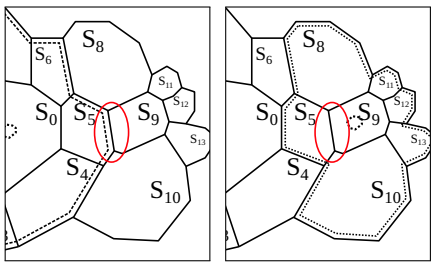

Figure 5: Updating segment boundaries. **(a)** Highlighted edge (red) will be fixed when processing the ring centered at S_0. **(b)** The same edge will be updated when processing the ring centered at S_9.

segmentation to neighboring slices, repeating this propagation until all slices are segmented. In practice, the global grain topology is largely consistent from one slice to its neighbors, but local topology may change due the appearance of a new grain or disappearance of an existing grain. Previous work [18] has shown that enforcing the topology in grain segmentation using the algorithm described in Section 3.1 on the entire image, followed by a local relabeling to accommodate local topology changes, can combine both global topology consistency and local topology inconsistency, and leads to improved segmentation performance. As discussed above, this cannot preserve the full inter-segment topology. In this experiment, we use the proposed method to propagate segmentation by enforcing full topology preservation, followed by the same local relabeling algorithm developed in [18], to segment the 3D metallic image volumes. We compare our performance with the algorithm developed in [18] and several other methods.

4.1. β-Ti grains in Ti-21S

We evaluate the proposed method on a sequence of 11 microscopic 750 px×525 px images consisting of β-Ti grains which are extracted from a Ti-21S titanium materials volume [14]. We additionally have a ground-truth for these slices, created by materials scientists, for performance evaluation.

We first validate that the 2D slices of such grain images contain many ring structures. On the ground-truth segmentation, we take each segment as the center, combined with all its adjacent segments, and check whether such a local structure is a ring. Experiments show that out of 5586 local structures across all slices, we have 5202 (93%) ring structures. Sample non-ring structures are shown in Fig. 6. Such non-ring structures usually contain a very small non-center segment that does not reach the ring boundary and, for such non-ring structures, we simply apply the same algorithm described in Section 3 to update its segmentation. While the topology is not strictly preserved, the effect on

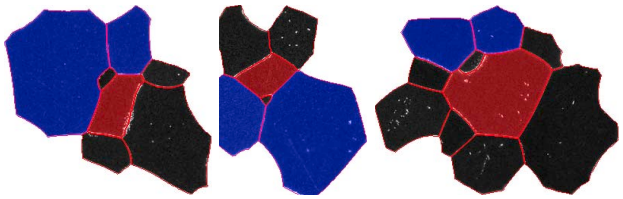

Figure 6: Sample non-ring local structures (center segment in red).

the final performance is minimal since these cases are only a small percentage of the total updated local structures. Furthermore, these small structures are more likely to undergo local topology changes, and it is therefore less important or desirable to enforce a fixed topology in these instances.

We evaluate the proposed method by selecting one slice as the initial template and propagating its ground-truth segmentation to the other 10 slices repeatedly. In turn, we use each of the 11 slices as the initial template to segment the other 10 slices. This way, on each slice, we obtain 10 segmentation results (omitting the runs where the slice was used as the initial template). We compare each segmentation result with the corresponding ground-truth segmentation, find the edge pixel coincidence (within a 3 px tolerance), and calculate the precision/recall and the combined F-measure. On each slice, we calculate the mean and standard deviation of the precision, recall, and F-measure over the 10 segmentation results, which are shown in Fig. 7. We also measure the segment-number difference between the segmentation result and the ground truth, which we call the *cardinality difference*: positive values indicate undersegmentation, and negative values indicate oversegmentation. The cardinality difference on each slice (mean and standard deviation) are shown in Fig. 7 (d). Finally, in Fig. 8, we show the total MRF energy in the proposed algorithm converges, since the energy decreases after each ring structure is processed.

For comparison, we run the MATLAB implementation of the watershed method [12], and the linear-time multiscale normalized cut method [5], on the same 11 image slices. For watershed, we use a propagation strategy of the same form as in the proposed method, where we initialize the markers for watershed with an eroded version of the segmentation on the previous slice. For the normalized cut method, we provide the ground-truth number of segments for all slices. In addition, we compare with the method from [18], which attempts to preserve the topology by applying graph cut over the entire image. As mentioned above, for both proposed method and the method in [18], we include an identical local-relabeling step [18] to accommodate possible local topology changes resulting from newly appearing or disappearing grains between slices.

Figure 7 shows the results of this experiment. The proposed method is competitive with the comparison methods

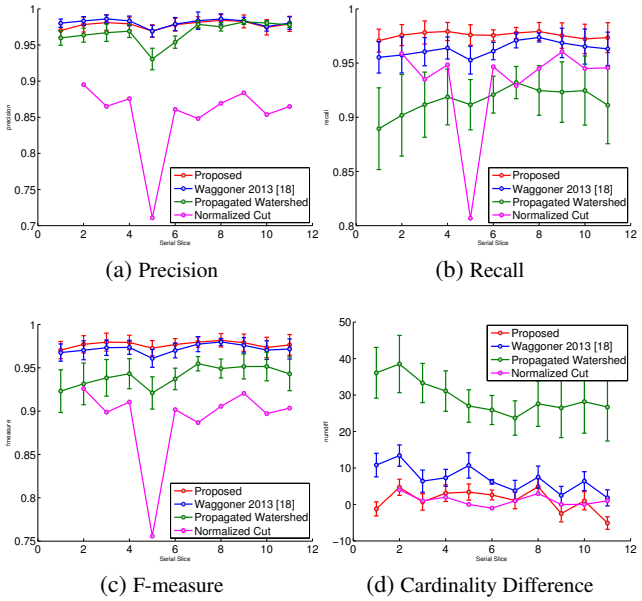

(a) Precision (b) Recall

(c) F-measure (d) Cardinality Difference

Figure 7: Performance of the proposed method, the previous topology-preserving image segmentation method [18], a propagated watershed method, and the normalized cut method, on the Ti-26S dataset.

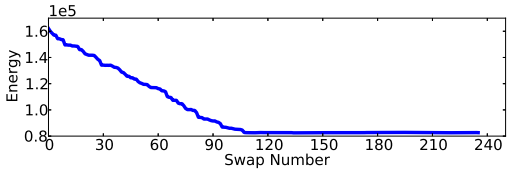

Figure 8: Total energy (y-axis) as each local ring structure is processed (x-axis) on a representative slice from the Ti-26S dataset.

as shown from the precision score in Fig. 7 (a), and performs better than other methods in recall and the overall F-measure (Fig. 7 (b) and Fig. 7 (c)). Also of note, the proposed method obtains closer to the correct number of segments, shown by the cardinality difference measure in Fig. 7 (d), where other competing methods tend to undersegment the slices. The normalized cut method is comparable to the proposed method for the cardinality difference measure, however, it is given the number of ground-truth slices as its input, so it is expected to obtain a near-ideal cardinality difference score.

Qualitative results are shown in Fig. 9 (a). The proposed method is clearly competitive with the method in [18] and the watershed method. The watershed method tends to undersegment slightly, while normalized cut places the correct number of segments (since it is given this as input), but fails to find the correct segment boundaries in many instances. Because the proposed method and the method in [18] show similar performance in the high-level view in Fig. 9 (a), we further show the more subtle differences between these two methods in Fig. 9 (b). Notice that the proposed method correctly captures the grain boundaries more often, and captures them more accurately during the propagation, which leads to its better quantitative score in Figure 7.

These experiments were conducted on a 2GHz Linux workstation with 8GB of memory. The proposed method is implemented in Python, with specific hotspots optimized in C. The proposed method requires less than 5 minutes per propagation, while the relabeling process from [18], implemented in C++, adds an additional 8 minutes. This is commensurate with the propagation time reported by the comparison method in [18].

4.2. DREAM3D Volumes

Since we have only a limited number of slices for the Ti-21S material, we expand our evaluation by including synthetic volumes created using DREAM3D [8]. DREAM3D (Digital Representation Environment for Analyzing Microstructure in 3D) is a tool created by materials scientists specifically to aid in the creation, reconstruction, and analysis of 3D materials volumes, and provides a variety of tools, including a synthetic volume builder which we use to create realistic, physically-based synthetic materials volumes for our evaluation. The four synthetic volumes generated for our experiment are shown in Fig. 10 with detailed information shown in Table 1.

In generating these synthetic datasets, we add realistic simulated noise in the grain and along the grain boundary, and random scratches within the grain, and across entire slices, as shown in Fig. 11. The noise parameters were directly sampled from the Ti-26S dataset, which is a common practice in the materials community for generating large datasets. We generate the DREAM3D volumes with roughly the same inter-slice spacing as in the Ti-26S dataset so we can use comparable same algorithm settings.

From Fig. 12, the proposed method again performs better overall on the DREAM3D-created volumes compared to other comparison methods. Particularly, for image volume (d), a single template segmentation is propagated as far as 150 slices and the proposed method is still able to achieve an F-measure of 0.85.

4.3. Interactive and Stereo Applications

To illustrate the general usefulness of this approach, we use the proposed method to segment a selection of natural and biological images. We use an interactive segmentation approach where the user annotates each object in the image with 1-2 clicks, and we infer the inter-segment topology from the Voronoi tessellation of the selected points, allowing the user to refine the points until the inferred topology is correct. This can be taken as the initialization for segmentation using the proposed method. Final segmentations are shown in the first three rows of Fig. 13.

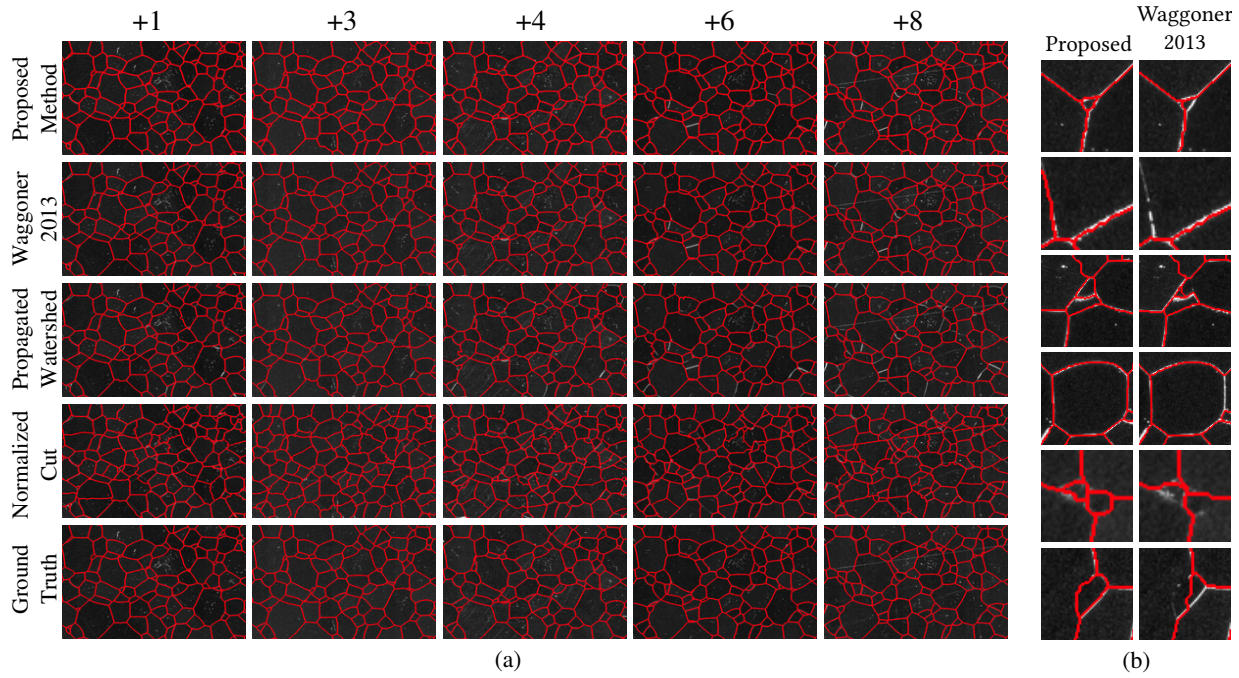

Figure 9: **(a)** Qualitative results for the Ti-26S dataset for the proposed method, the method in [18], the propagated watershed method, and normalized cut. The distance from the initial template is shown by the numbers along the top. **(b)** The more subtle differences between the proposed method and the method in [18].

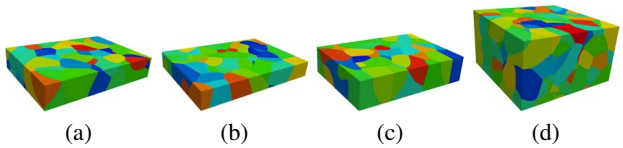

Figure 10: Synthetic volumes generated by DREAM3D [8].

Vol	Dimensions	Imaged Size (voxels)
(a)	$22.5\,\mu m \times 15.75\,\mu m \times 4\,\mu m$	$750 \times 525 \times 50$
(b)	$22.5\,\mu m \times 15.75\,\mu m \times 3\,\mu m$	$750 \times 525 \times 50$
(c)	$22.5\,\mu m \times 15.75\,\mu m \times 5\,\mu m$	$750 \times 525 \times 50$
(d)	$37.5\,\mu m \times 36.75\,\mu m \times 10.5\,\mu m$	$750 \times 525 \times 150$

Table 1: Dimensions of the synthetic datasets, and their imaged resolution on which the noise model is applied.

Similar to the propagation approach discussed previously, we can use the proposed method to propagate a segmentation between two images collected for stereo matching. As before, we provide a segmentation of one of the images, and use this as the initialization to segment the other image. Results are shown in the last two rows of Fig. 13.

5. Conclusion

We have presented a new method for propagating a multi-label segmentation from one image to another by preserving both inter-segment topology and intra-segment topology. The former requires the specified segment adjacency relations and the latter requires the connectivity of each segment. We showed that this can be accomplished when each segment and its adjacent segments constitute a ring structure. We developed a multi-labeling approach preserve these two types of topology within the MRF framework, applied the proposed method to segment 3D metallic images for underlying grain structures, and achieved better performance than several comparison methods.

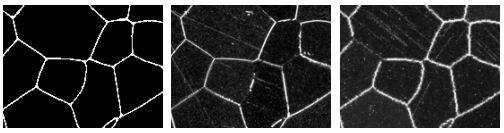

Figure 11: Comparison of a real slice and the noise model applied to the ground truth.

Acknowledgments This work was supported by AFOSR FA9550-11-1-0327 and NSF IIS-1017199.

References

[1] R. K. Ahuja, T. L. Magnanti, and J. B. Orlin. *Network Flows: Theory, Algorithms, & Applications*. Prentice Hall, Englewood Cliffs, NJ,

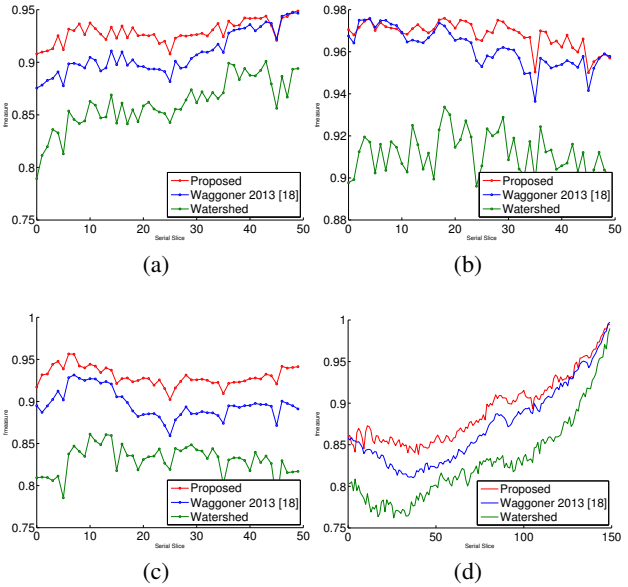

Figure 12: Performance on the DREAM3D generated datasets; (a)-(d) correspond with Table 1 and Fig. 10, (a)-(c) show the average F-measure by taking different slices as the initial template, and (d) shows the F-measure from a single round of propagation starting with slice 150 as the initial template.

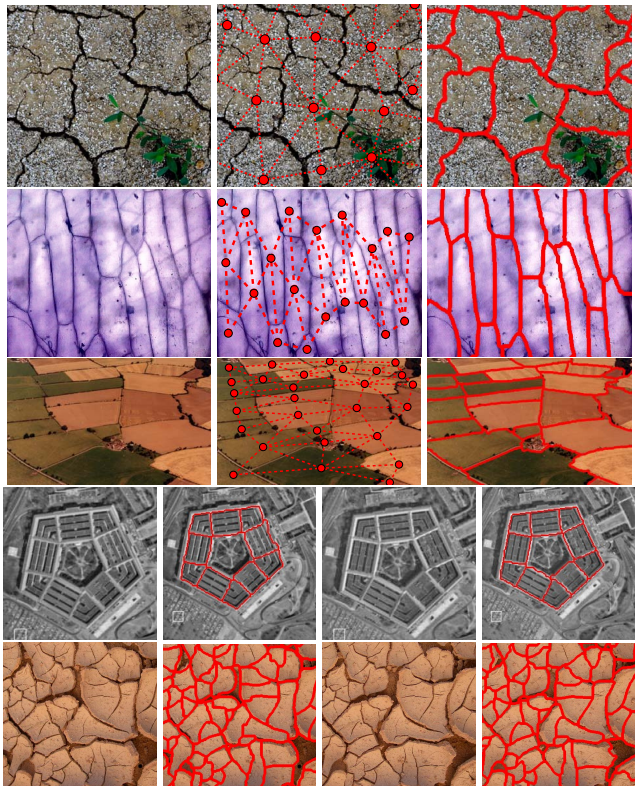

Figure 13: Qualitative segmentation results on natural and biological images. All images obtained from Flickr or Google Images. **(Rows 1-3)** Interactive segmentation on cracked dirt, onion cells, and aerial photography, respectively. The first column shows the original image, the second column displays the region adjacency graph derived from the Voronoi tessellation of the selected points, and the third column shows the resulting segmentation. **(Rows 4-5)** Segmentation propagation between two images collected for stereo matching, of aerial phtography and cracked ground tiles, respectively. The left two columns show the first image and its segmentation, and the right two columns show the second image and its resulting segmentation which is propagated from the first image.

1993. 3

[2] Y. Boykov and M. Jolly. Interactive graph cuts for optimal boundary & region segmentation of objects in nd images. In *ICCV*, volume 1, pages 105–112. IEEE, 2001. 3

[3] Y. Cao, L. Ju, Q. Zou, C. Qu, and S. Wang. A multichannel edge-weighted centroidal voronoi tessellation algorithm for 3D super-alloy image segmentation. In *CVPR*, pages 17–24, 2011. 1

[4] C. Chen, D. Freedman, and C. H. Lampert. Enforcing topological constraints in random field image segmentation. In *CVPR*, 2011. 1, 2

[5] T. Cour, F. Benezit, and J. Shi. Spectral segmentation with multiscale graph decomposition. In *CVPR*, pages 1124–1131, 2005. 5

[6] J. Cousty, G. Bertrand, L. Najman, and M. Couprie. Watershed cuts: Thinnings, shortest path forests, and topological watersheds. *TPAMI*, 32(5):925 –939, 2010. 1, 2

[7] X. Han, C. Xu, and J. L. Prince. A topology preserving deformable model using level set. In *CVPR*, volume 2, pages 765–770, 2001. 1, 2

[8] M. Jackson and M. Groeber. DREAM3D. `http://dream3d.bluequartz.net` , 2012. 6, 7

[9] V. Jain, B. Bollmann, M. Richardson, et al. Boundary learning by optimization with topological constraints. In *CVPR*, pages 2488–2495, June 2010. 1, 2

[10] D. Letscher and J. Fritts. Image segmentation using topological persistence. In *CAIP*, pages 587–595, 2007. 1, 2

[11] T. Mcinemey and D. Terzopoulos. Topology adaptive deformable surfaces for medical image volume segmentation. *TMI*, 18(10):840–850, 1999. 1

[12] F. Meyer. Topographic distance and watershed lines. *Signal Processing*, 38(1):113–125, 1994. 5

[13] S. Nowozin and C. H. Lampert. Global connectivity potentials for random field models. In *CVPR*, pages 818–825. IEEE, 2009. 1, 2

[14] D. Rowenhorst, A. Lewis, and G. Spanos. Three-dimensional analysis of grain topology and interface curvature in a β-titanium alloy. *Acta Materialia*, 58:5511–5519, 2010. 1, 5

[15] R. Szeliski, D. Tonnesen, and D. Terzopoulos. Modeling surfaces of arbitrary topology with dynamic particles. In *CVPR*, pages 140–152, 1993. 1

[16] O. Veksler. *Efficient graph-based energy minimization methods in computer vision*. PhD thesis, Cornell University, Ithaca, NY, USA, 1999. 2, 4

[17] S. Vicente, V. Kolmogorov, and C. Rother. Graph cut based image segmentation with connectivity priors. *CVPR*, 0:1–8, 2008. 1, 2

[18] J. Waggoner, Y. Zhou, J. Simmons, M. D. Graef, and S. Wang. 3D materials image segmentation by 2D propagation: A graph-cut approach considering homomorphism. *IEEE Transactions on Image Processing*, 22:5282–5293, 2013. 2, 3, 5, 6, 7

[19] Y. Zeng, D. Samaras, W. Chen, and Q. Peng. Topology cuts: A novel min-cut/max-flow algorithm for topology preserving segmentation in N-D images. *CVIU*, 112(1):81–90, Oct. 2008. 1, 2

[20] Y. Zhang and T. Chen. Efficient inference for fully-connected CRFs with stationarity. In *CVPR*, pages 582–589, 2012. 1, 2